Journal of Materials Chemistry A

ROYAL SOCIETY OF CHEMISTRY

PAPER

View Article Online
View Journal | View Issue

Cite this: J. Mater. Chem. A, 2024, 12, 20247

Long-wavelength photoresponsive gallium zinc oxynitride for efficient oxygen evolution and Z-scheme water splitting reactions†

Natsutogi Iwasa,‡[a] Hiroka Sandaiji,‡[b] Swarnava Nandy,[c] Mamiko Nakabayashi,[d] Tsuyoshi Takata,[c] Takashi Hisatomi *[cef] and Kazunari Domen *[cfgh]

Received 23rd May 2024
Accepted 28th June 2024

DOI: 10.1039/d4ta03576c

rsc.li/materials-a

Long-wavelength photoresponsive GaN:ZnO, a solid solution of GaN and ZnO, can be obtained by reacting Ga_2O_3 and Zn_3N_2 in the presence of ZnX_2 (X = halogen) in a sealed evacuated tube. However, the activity of GaN:ZnO for overall water splitting *via* one-step excitation under visible light remains low due to the small particle size, which leads to uncontrollable aggregation and lack of suitable cocatalysts. In this study, well-dispersed particulate GaN:ZnO with a ZnO concentration of 66 mol%, optical absorption up to about 600 nm, and anisotropic crystalline facets was obtained using δ-Ga_2O_3 as a raw material and adding Zn to the starting material. The resulting GaN:ZnO exhibited an apparent quantum yield of 11.9% at 420 nm in the oxygen evolution reaction when loaded with an IrO_x cocatalyst. It also served as an oxygen evolution photocatalyst in a photocatalyst sheet for Z-scheme water splitting, in combination with $La_5Ti_2Cu_{0.9}Ag_{0.1}O_7S_5$, whose absorption edge wavelength was about 700 nm, as a hydrogen evolution photocatalyst. This work, which demonstrates the activation of long-wavelength photoresponsive GaN:ZnO, expands the possibilities of constructing photocatalytic systems that effectively utilize long-wavelength visible light for water splitting.

Introduction

Large-scale implementation of solar fuel production is desired in order to address increasingly serious energy and environmental problems.[1] Sunlight-driven water splitting using particulate semiconductor photocatalysts has been studied as a means of green hydrogen production on a large scale.[2–4] To produce green hydrogen in a practical manner, it is indispensable to develop photocatalytic materials that can efficiently split water into hydrogen and oxygen under long-wavelength visible light.[5] Various semiconducting (oxy)nitrides, oxysulphides and metal-doped oxides have been extensively studied as visible-light responsive photocatalysts.[6–9] Despite having a narrower bandgap than the corresponding pure oxides, many such materials have a band structure suitable for splitting water into hydrogen and oxygen under visible-light irradiation. This is due to a negative shift of the valence band edge potential induced by nitride and sulphide ions or impurity levels associated with dopants, while the conduction band edge potential is largely unaffected.

GaN:ZnO is one of the earliest oxynitride photocatalysts shown to be capable of splitting water into hydrogen and oxygen under visible light.[10] The bandgap energy of GaN:ZnO can be controlled by the concentration of ZnO. With increasing ZnO concentration up to 90 mol%, the valence band maximum shifts negatively while the conduction band minimum shifts positively.[11] In 2010, an apparent quantum yield (AQY) of 5.1% at 410 nm was achieved in the overall water splitting reaction using GaN:ZnO with a ZnO concentration of 13 mol% and an absorption edge wavelength of about 480 nm.[12] More recently, in 2022, GaN:ZnO with an absorption edge wavelength of around 550 nm and activity in the water splitting reaction was synthesised by applying NH_4Cl as a solid nitrogen source in a sealed evacuated tube.[13] The activity of the resultant long-wavelength responsive GaN:ZnO for overall water splitting was rather low, with a solar-to-hydrogen energy conversion efficiency (STH efficiency) on the order of 1×10^{-2}%. Nevertheless, GaN:ZnO could be effectively applied to visible-light-driven

[a]Department of Science and Technology, Graduate School of Medicine, Science and Technology, Shinshu University, Nagano 380-8553, Japan
[b]Department of Engineering, Graduate School of Science and Technology, Shinshu University, Nagano 380-8553, Japan
[c]Research Initiative for Supra-Materials (RISM), Shinshu University, Nagano 380-8553, Japan. E-mail: hisatomi@shinshu-u.ac.jp; domen@shinshu-u.ac.jp
[d]Institute of Engineering Innovation, School of Engineering, The University of Tokyo, Tokyo 113-8656, Japan
[e]Precursory Research for Embryonic Science and Technology (PRESTO), Japan Science and Technology Agency (JST), Nagano 380-8553, Japan
[f]Institute for Aqua Regeneration, Shinshu University, Nagano 380-8553, Japan
[g]Office of University Professors, The University of Tokyo, Tokyo 113-8656, Japan
[h]Department of Chemistry, Kyung Hee University, Seoul, 130-701, Republic of Korea

† Electronic supplementary information (ESI) available. See DOI: https://doi.org/10.1039/d4ta03576c

‡ These authors have contributed equally.

water splitting by constructing a Z-scheme system using two-step excitation of a hydrogen evolution photocatalyst (HEP) and an oxygen evolution photocatalyst (OEP). Namely, GaN:ZnO effectively functioned as the OEP in combination with Rh-doped $SrTiO_3$ as the HEP in the presence of Fe^{3+}/Fe^{2+} as the redox mediator, and the resulting Z-scheme system split water with a higher STH efficiency of 3.7×10^{-2}%. The use of long-wavelength photoresponsive GaN:ZnO allowed the wavelength range of light applicable to Z-scheme water splitting reactions to be significantly extended, because most previous work had used WO_3 and $BiVO_4$ as OEPs for Z-scheme water splitting, whose absorption edge wavelengths were rather short, at 470 and 525 nm, respectively.[14,15]

Further improvements in efficiency can be expected by optimizing the performance of GaN:ZnO. At the same time, it is still essential to explore new long-wavelength HEP materials, because Rh-doped $SrTiO_3$ can utilise visible light only up to 520 nm, and its visible-light absorption induced by the Rh impurity level is rather weak.[16]

In our recent study, GaN:ZnO absorbing visible light up to 580 nm was synthesized by reacting crystalline Ga_2O_3 and Zn_3N_2 in the presence of ZnX_2 (X = halogen) in sealed evacuated tubes.[17] The use of hydrogen-free Zn_3N_2 as a nitriding reagent allowed gram-scale synthesis of GaN:ZnO that was active for overall water splitting *via* one-step photoexcitation. However, the AQY remained on the order of 1×10^{-2}% at a wavelength of 430 nm. This low activity is due to the uncontrolled particle size and morphology of GaN:ZnO, resulting in severe aggregation, which makes it difficult to refine the cocatalyst loading.

In general, the properties of the products of solid-state reactions are affected by the particle size and crystallinity of the reactants.[18] Therefore, refinement of the raw materials is expected to lead to improved morphology control and photocatalytic activity of GaN:ZnO obtained using Zn_3N_2 as a solid nitrogen source. In the present study, well-dispersed crystalline GaN:ZnO particles with a high ZnO concentration were synthesised using δ-Ga_2O_3 as a raw material and adding Zn to the starting materials. The particles absorbed visible light up to 600 nm and exposed hexagonal crystalline facets. The resulting GaN:ZnO drove the oxygen evolution reaction with an AQY of 11.9% at 420 nm when loaded with an IrO_x cocatalyst. When used in combination with $La_5Ti_2Cu_{0.9}Ag_{0.1}O_7S_5$ (LTCA) as a HEP, it also enabled a Z-scheme system consisting only of non-oxide photocatalysts with an absorption edge wavelength equal to or longer than 600 nm, but still active in visible light-driven water splitting.

Results and discussion

Synthesis of GaN:ZnO

Fig. S1A in ESI† shows XRD patterns for the δ- and K-Ga_2O_3 samples. The pattern for the δ-Ga_2O_3 sample is consistent with that reported in the literature.[19] The synthesised δ-Ga_2O_3 particles were aggregated to form irregularly shaped secondary particles (Fig. S1B in ESI†). TGA measurements revealed that the δ-Ga_2O_3 sample contained about 8 wt% water, as indicated by the weight loss associated with endothermic signals during the heating process (Fig. S2 in ESI†). On the other hand, the K-Ga_2O_3 was composed of a mixture of α-Ga_2O_3 and β-Ga_2O_3. The K-Ga_2O_3 particles had a high-aspect-ratio rectangular parallelepiped shape with a length of several micrometers and a thickness of less than 1 μm. The K-Ga_2O_3 contained a negligible amount of water. Fig. 1A and B respectively show XRD patterns and UV-vis DRS data for GaN:ZnO synthesised using δ- and K-Ga_2O_3 as a starting material with and without addition of Zn after washing with distilled water. The washing step was performed to investigate byproducts of the synthesis of GaN:ZnO. Single-phase GaN:ZnO was obtained from K-Ga_2O_3, while a small amount of $ZnGa_2O_4$ was generated as an impurity phase, as confirmed by the diffraction peak at 36.8°, when δ-Ga_2O_3 was used. This is due to oxidation of Zn_3N_2 by the moisture contained in δ-Ga_2O_3. The addition of metallic Zn to the precursor mixture prevented the formation of $ZnGa_2O_4$, because Zn reacted with moisture to form ZnO and H_2 in the sealed quartz tube. On the other hand, unreacted Zn remained when Zn was added to the synthesis using K-Ga_2O_3. GaN:ZnO(δ) prepared with Zn addition had similar crystallinity to GaN:ZnO(K), but exhibited diffraction peaks at lower angles closer to those for ZnO than GaN, indicating the production of GaN:ZnO with a higher ZnO concentration. In fact, the ZnO concentration estimated from the Zn/Ga ratio measured by EDS analysis was higher for GaN:ZnO(δ) prepared with Zn addition (63 mol%) than for GaN:ZnO(K) prepared with or without Zn addition (58 mol% for both). The higher ZnO concentration in the former case indicates that ZnO generated from Zn and moisture was partially incorporated in the GaN:ZnO(δ) product. In accordance with this, the GaN:ZnO(δ) sample prepared with Zn absorbed visible light up to 600 nm, which was approximately 30 nm longer than the absorption edge for GaN:ZnO(K). Note that when commercial submicron ZnO particles were added instead of Zn for the synthesis of GaN:ZnO(δ), the XRD peak for the product was not shifted relative to that for conventional

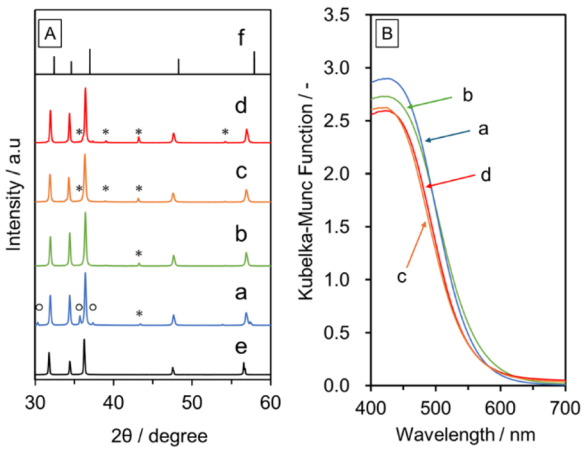

Fig. 1 (A) XRD patterns (B) UV-vis DRS data for GaN:ZnO prepared using (a) δ-Ga_2O_3, (b) δ-Ga_2O_3 with addition of Zn, (c) K-Ga_2O_3 and (d) K-Ga_2O_3 with addition of Zn by heating at 1173 K for 10 h. (e) and (f) Show XRD patterns for commercial ZnO and GaN (ICDD: 00-050-792), respectively, for comparison. Peaks for Zn and $ZnGa_2O_4$ are indicated with asterisks (*) and circles (○), respectively.

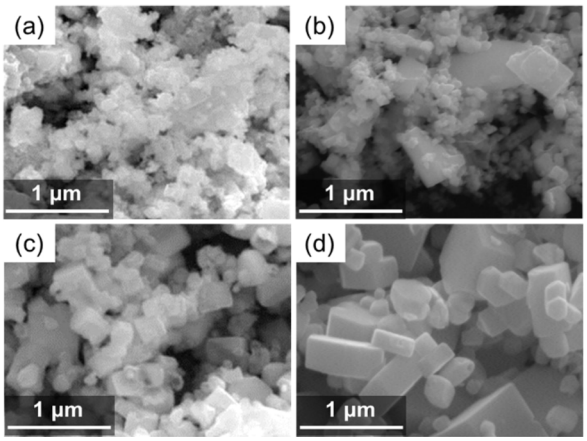

Fig. 2 SEM images of (a and b) GaN:ZnO(K) and (c and d) GaN:ZnO(δ) prepared by heating at 1173 K for 10 h (a and c) without and (b and d) with Zn addition.

GaN:ZnO(K), and instead XRD peaks attributable to ZnO were generated, indicating that externally added ZnO was not incorporated into GaN:ZnO (Fig. S3†).

Fig. 2 shows SEM images of GaN:ZnO(δ) and GaN:ZnO(K) synthesised with and without Zn addition. The morphology and size of the GaN:ZnO(K) particles are not very clear or uniform regardless of the addition of Zn during synthesis. In contrast, hexagonal prismatic particles reflecting the wurtzite-type crystal structure of GaN:ZnO are observed when δ-Ga_2O_3 is used because Ga_2O_3 can be more smoothly converted into GaN:ZnO. This effect is enhanced by the addition of Zn to the starting material, and allows GaN:ZnO(δ) particles to grow. This is probably related to suppression of oxidation and hydrolysis of the starting Zn_3N_2 and the intermediate Zn_2NI, as described later.

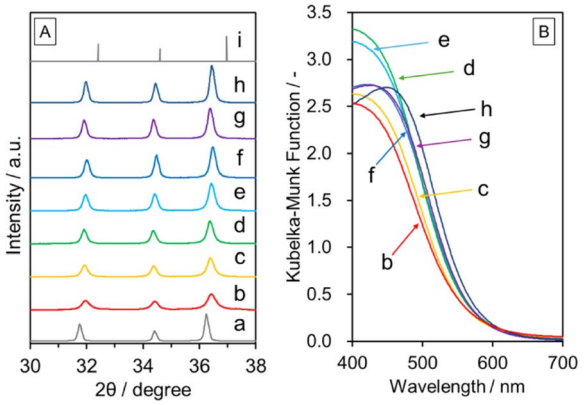

Fig. 3 (A) XRD and (B) DRS data for GaN:ZnO(δ) prepared with Zn addition at (b) 923, (c) 973, (d) 1023, (e) 1073, (f) 1123, (g) 1173, and (h) 1223 K for 10 h. (a) and (i) Show peaks for commercial ZnO and GaN (ICDD: 00-050-792), respectively, for comparison.

Fig. 3 shows XRD and DRS data for GaN:ZnO(δ) prepared at different temperatures. All the synthesized samples were attributed to single-phase wurtzite-type GaN:ZnO. It can be seen that the diffraction peaks become sharper as the synthesis temperature is increased, indicating an improvement in crystallinity. Namely, the full width at half maximum (FWHM) values for the 101 diffraction peak for GaN:ZnO(δ) synthesised at 923 and 1123 K are 0.35° and 0.17°, respectively. At temperatures above 1123 K, the FWHM is largely unchanged. The onset of optical absorption observed in the DRS data was around 600 nm regardless of the synthesis temperature, and was approximately 30 nm longer than that for GaN:ZnO(K). This reflects a higher ZnO concentration in the GaN:ZnO(δ) samples due to the incorporation of ZnO generated *in situ* from Zn and H_2O during synthesis. In fact, elemental analysis revealed that the ZnO concentration in the GaN:ZnO(δ) samples was around 65 mol% (Table 1), while that for GaN:ZnO(K) reported in our previous work was 58 mol%.[17]

SEM images of GaN:ZnO(δ) synthesized at different temperatures are shown in Fig. 4. GaN:ZnO(δ) synthesised at 923 K was composed of particles smaller than 100 nm without noticeable crystal facets. Increasing the synthesis temperature led to the growth of particles with some crystal facets, and well-dispersed hexagonal prismatic particles reflecting the crystal structure and hundreds of nanometers in size were generated at 1073 K and above. Note that GaN:ZnO with such anisotropic particle shapes can also be synthesised using K-Ga_2O_3 instead of δ-Ga_2O_3 when Zn_2NI is used as the zinc and nitride ion source.[17] In fact, Zn_2NI is generated *in situ* from Zn_3N_2 and ZnI_2 during the synthesis of GaN:ZnO. However, Zn_3N_2 is prone to oxidation and hydrolysis. In addition, Zn_2NI starts to decompose at 873 K to Zn, N_2, and ZnI_2, which are no longer reactive enough to form GaN:ZnO.[20] The use of δ-Ga_2O_3, which is more reactive than K-Ga_2O_3, is therefore preferable for the growth of hexagonal prismatic particles of GaN:ZnO, as the decomposition of Zn_2NX into inert byproducts prior to the formation of GaN:ZnO can be suppressed. Notably, Pt and MnO_x were reductively and oxidatively photodeposited respectively on the hexagonal and lateral planes of hexagonal prismatic particles of GaN:ZnO (Fig. S4 in ESI†). This indicates a spontaneous polarisation of GaN:ZnO like GaN and ZnO.[21–23]

Table 1 Bulk composition of GaN:ZnO(δ) prepared at different temperatures

Synthesis temperature/K	Ga/wt%[a]	Zn/wt%[a]	N/wt%[b]	O/wt%[b]	Total/wt%	Composition
1073	28.3	49.6	5.8	13.0	96.7	$Ga_{0.35}Zn_{0.65}N_{0.35}O_{0.67}$
1123	28.4	50.1	5.7	12.8	97.0	$Ga_{0.35}Zn_{0.65}N_{0.34}O_{0.66}$
1173	28.5	50.8	5.7	12.9	97.9	$Ga_{0.34}Zn_{0.66}N_{0.34}O_{0.66}$
1223	28.0	49.6	5.8	13.2	96.6	$Ga_{0.35}Zn_{0.65}N_{0.33}O_{0.67}$

[a] Measured by ICP-AES. [b] Measured by N/O combustion analysis.

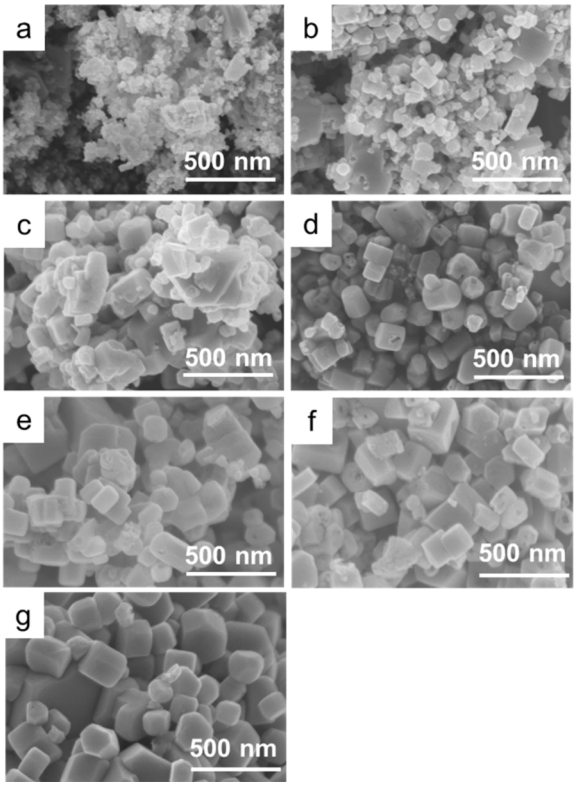

Fig. 4 SEM images of GaN:ZnO(δ) synthesised with addition of Zn at (a) 923, (b) 973, (c) 1023, (d) 1073, (e) 1123, (f) 1173, and (g) 1223 K.

A transmission electron microscopy (TEM) image and electron diffraction patterns for GaN:ZnO(δ) synthesised at 1173 K are shown in Fig. 5. The electron diffraction patterns obtained at different positions in the particle shown in the TEM image are similar, indicating that the GaN:ZnO(δ) particle is a single crystal. Considering the results of the elemental analysis (Table 1), the GaN:ZnO(δ) material is also stoichiometric. Nevertheless, as seen in the TEM image, the GaN:ZnO(δ) particle contains internal voids suggesting the presence of local defects and distortions.

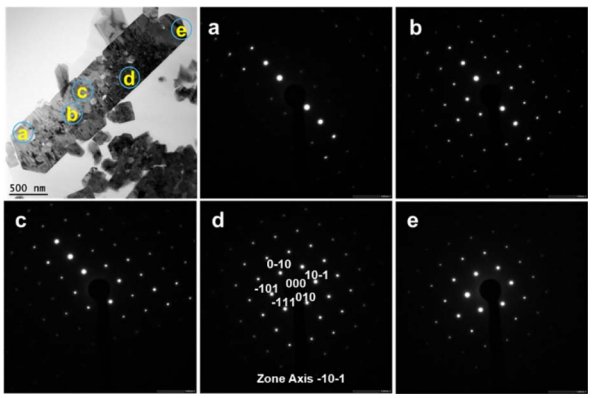

Fig. 5 Cross-sectional TEM image and (a–e) selected area electron diffraction patterns for GaN:ZnO(δ) synthesised at 1173 K for 10 h. The positions where the diffraction patterns were acquired are labelled with letters a to e.

Photocatalytic water splitting reaction

Fig. 6 shows the oxygen evolution activity under visible light in an aqueous $AgNO_3$ solution for GaN:ZnO(δ) synthesised at 973–1223 K and loaded with IrO_x (0.5 wt% Ir). The activity is seen to increase as the synthesis temperature is raised from 973 to 1173 K due to improvements in crystallinity. However, the activity for the sample synthesised at 1223 K decreases even though there is no appreciable deterioration in crystallinity or bulk composition. This may be related to a change in the surface properties of GaN:ZnO(δ). In fact, when GaN:ZnO was synthesized at high temperature using NH_4Cl as a nitriding reagent, a decrease in the surface Zn/Ga ratio was observed, and the photocatalytic activity was eventually degraded.[13] XPS analysis of GaN:ZnO(δ) was therefore carried out. Fig. S5 and Table S1 in ESI† show the surface composition of GaN:ZnO(δ) prepared at different temperatures. GaN:ZnO(δ) synthesised at 1223 K showed a higher Zn/Ga molar ratio on the surface than the other GaN:ZnO samples, probably due to the heating at too high a temperature in an oxygen-free atmosphere for this material. The large deviation between the bulk and surface compositions would disturb the band structure and carrier transfer, which could lower the photocatalytic activity. As seen in Fig. S6 in ESI,† the oxygen evolution activity for GaN:ZnO(δ) decreases to about 20% in the absence of an IrO_x cocatalyst, indicating that the IrO_x acts as an efficient oxygen evolution cocatalyst as reported previously.[13] The oxygen evolution activity is almost constant for an Ir loading of 0.2 wt% or greater. The wavelength dependence of the AQY for the most active IrO_x-GaN:ZnO(δ) sample, which was synthesised at 1173 K and loaded with 0.5 wt% of Ir, for the oxygen evolution reaction is presented in Fig. 7. As can be seen, the AQY at a wavelength of 420 nm is 11.9%, which is comparable to that for GaN:ZnO synthesised using NH_4Cl as a solid

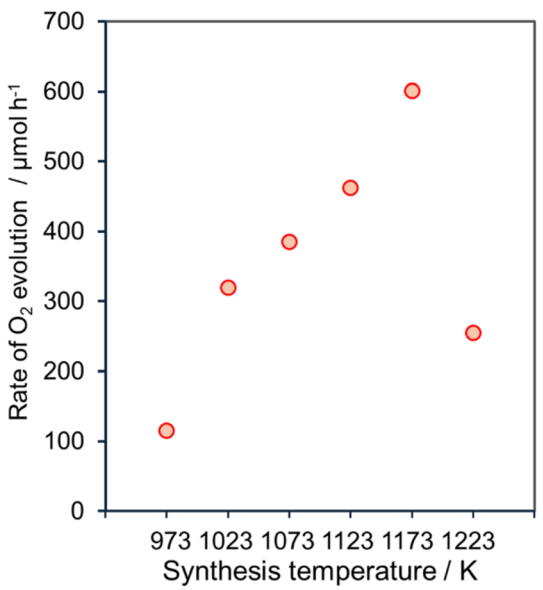

Fig. 6 Oxygen evolution activity in aqueous $AgNO_3$ solution (30 mM) for IrO_x-GaN:ZnO(δ) synthesised at different temperatures. The reactions were carried out under visible light irradiation (λ > 420 nm) from a 300 W Xe lamp. The amount of IrO_x loading was 0.5 wt%.

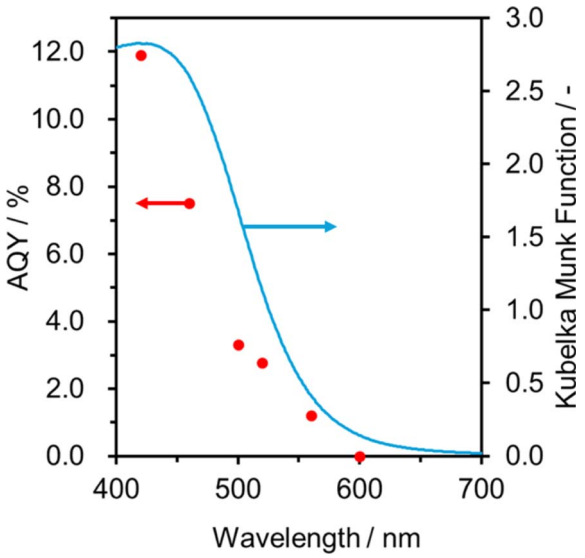

Fig. 7 AQY for GaN:ZnO(δ) synthesised at 1173 K and loaded with IrO_x (Ir 0.5 wt%) for oxygen evolution reaction as function of irradiation wavelength. The reactions were carried out in an aqueous $AgNO_3$ solution (30 mM) under illumination from a 300 W Xe lamp equipped with various bandpass filters.

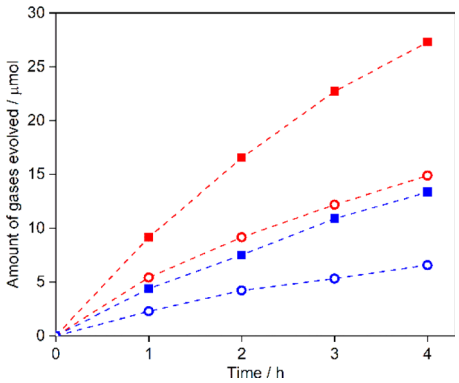

Fig. 8 Time course for H_2 (red) and O_2 (blue) gas evolution for photocatalyst sheets using unmodified GaN:ZnO (open circles) and IrO_x-loaded GaN:ZnO (closed squares) as the OEP in combination with LTCA and Au as the HEP and conductor layer, respectively, under visible light (λ > 420 nm).

nitrogen source, and outstanding among GaN:ZnO with high ZnO concentration (Table S2 in ESI†). Notably, the GaN:ZnO(δ) sample maintains a reasonably high AQY of 1% at a wavelength of 560 nm, but its activity becomes negligible under irradiation with monochromatic light at 600 nm, which represents the absorption edge. This suggests that the photocatalytic reaction proceeds through bandgap transitions of GaN:ZnO(δ) and that visible light absorption up to 600 nm can indeed contribute to the photocatalytic activity. On the other hand, GaN:ZnO(δ) prepared at 1123 K showed negligible hydrogen evolution activity from aqueous methanol solution although it generated hydrogen from aqueous ascorbic acid solution (Fig. S7 in ESI†). In previous studies, the conduction band minimum and valence band maximum for GaN:ZnO with a ZnO concentration of 50–68 mol% have been estimated to be in the range of −0.58 to −0.08 V *vs.* RHE and +1.80 to +2.47 V *vs.* RHE, respectively, with large variations probably due to differences in stoichiometry and homogeneity of the materials.[11,13,24] However, as the ZnO concentration increases, the energy offset between the conduction band minimum and the hydrogen evolution reaction potential decreases more than the energy offset between the valence band minimum and the oxygen evolution reaction potential, which may explain the low hydrogen evolution activity of GaN:ZnO(δ) in this work.

Since IrO_x-GaN:ZnO(δ) exhibited reasonably high activity in the oxygen evolution reaction in response to visible light with relatively long wavelengths, its applicability as an OEP for Z-scheme water splitting was investigated using a LTCA/Au/IrO_x-GaN:ZnO sheet. After photodeposition of Cr_2O_3/Rh cocatalysts, the sheet evolved H_2 and O_2 stoichiometrically under visible light from water free from sacrificial reagents or additives (Fig. 8). A sheet based on GaN:ZnO(δ) without IrO_x modification exhibited lower activity, indicating the critical role of the IrO_x cocatalyst in activating GaN:ZnO(δ). The STH efficiency for the sheet was 0.05% at 5 kPa and 310 K, which was an improvement on a previously reported $SrTiO_3$:Rh/$Fe^{3+/2+}$/GaN:ZnO suspension system, indicating the potential of achieving higher STH efficiency by using GaN:ZnO as the OEP in a sheet system.

Experimental

Preparation of GaN:ZnO

δ-Ga_2O_3 and Zn_3N_2 were synthesised as starting materials for GaN:ZnO in the laboratory. δ-Ga_2O_3 was prepared by calcining $Ga(NO_3)_3 \cdot xH_2O$ (Kojundo Chemical Laboratory Co., Ltd, 99.9%) at 573 K for 18 h in air.[19] The obtained white powder was crushed and again calcined at 573 K for 2 h. Zn_3N_2 was synthesized by heating commercial metallic Zn powder (Kojundo Chemical Laboratory Co., Ltd, particle size <75 μm, 99.9%) at 873 K for 10 h under an NH_3 flow at a rate of 100 mL min^{-1}.[17] δ-Ga_2O_3, Zn_3N_2, ZnI_2 (Sigma-Aldrich, 98%), and Zn were blended at a molar ratio of 1 : 1.1 : 2 : 1 in a N_2-filled glove box (dew point < 197 K, O_2 < 1 ppm), where Zn was added to prevent unwanted oxidation of the sample during heating. Commercially available Ga_2O_3 (Kojundo Chemical Laboratory Co., Ltd, 99.9%), denoted as K-Ga_2O_3, was also used to synthesise GaN:ZnO for comparison. The precursor mixture was transferred to a quartz tube, sealed under evacuation, and heated at 923–1273 K for 10 h. After heating, the sample was allowed to cool naturally to room temperature. The obtained GaN:ZnO powder was washed using 0.5 M HNO_3 for 1 h and thoroughly rinsed with distilled water to remove excess Zn and ZnI_2. The GaN:ZnO powder was recovered by filtration and dried overnight at 313 K in an oven. The sample was subsequently calcined in air at 873 K for 1 h to reduce the density of defects in the material and improve its photocatalytic activity.[25] The GaN:ZnO samples synthesized from δ-Ga_2O_3 and K-Ga_2O_3 are denoted as GaN:ZnO(δ) and GaN:ZnO(K), respectively.

The IrO_x cocatalysts (0.5 wt%) were loaded onto the surface of GaN:ZnO as an oxygen evolution cocatalyst by a solvothermal reaction using a microwave reactor (Monowave 200, Anton-

Paar). GaN:ZnO was dispersed in ethylene glycol containing $Na_3IrCl_6 \cdot nH_2O$ (Kanto Chemical, 99.5%), followed by heating at 423 K for 10 min.[7,13] The sample was washed with distilled water and recovered by filtration. The IrO_x-loaded GaN:ZnO powder was collected by filtration and dried at 313 K.

Rh was loaded onto IrO_x/GaN:ZnO by the photodeposition for the measurement of hydrogen evolution activity. The IrO_x/GaN:ZnO was suspended in a aqueous 10 mM ascorbic acid solution. To the suspension, $Na_3RhCl_6 \cdot nH_2O$ (Mitsuwa Chemicals, 18.3 wt% Rh) was added so that the fraction of Rh became 0.5 wt% with respect to the photocatalyst sample. The suspension was evacuated to completely remove dissolved air and then exposed to visible light ($\lambda \geq 420$ nm) from a Xe lamp equipped with a dichroic mirror and a cut-off filter.

To investigate the possibility of the facet-oriented electron/hole migration, Pt and MnO_x were reductively and oxidatively photodeposited on GaN:ZnO, respectively. Firstly, Pt (0.5 wt%) was loaded by reductive photodeposition. GaN:ZnO was dispersed in 10 vol% methanol solution containing $H_2PtCl_6 \cdot 6H_2O$ (Kanto Chemical Co., Inc., >98.5%), followed by irradiation with visible light ($\lambda \geq 420$ nm). Subsequently, MnO_x (Mn 0.5 wt%) was loaded by oxidative photodeposition. Pt-loaded GaN:ZnO was dispersed in 10 mM $NaIO_3$ solution containing $Mn(NO_3)_2 \cdot 6H_2O$ (Fujifilm Wako Pure Chemical Co., 98.0%), followed by irradiation with visible light ($\lambda \geq 420$ nm). The reactant solution was evacuated to remove air, and 10 kPa Ar was added prior to photodeposition.

Preparation of LTCA

Mg- and Al-codoped LTCA was synthesized by a conventional solid-state reaction in a sealed quartz tube similarly to a previous report.[26] TiO_2 (rutile, Kanto Chemical Co. Inc., 99.99%) was first impregnated with $Mg(NO_3)_2 \cdot 6H_2O$ (Fujifilm Wako Pure Chemical Co., 99.5%) and $Al(NO_3)_3 \cdot 9H_2O$ (Fujifilm Wako Pure Chemical Co., 99.5%) as Mg and Al dopant sources, respectively, and calcined at 1073 K for 1 h in air. The Mg (Mg^{-1} + Al + Ti) and Al/(Mg + Al + Ti) molar ratios were both 1%. The resulting material is denoted as Mg- and Al-codoped TiO_2. Before mixing with other chemicals, La_2O_3 (Kanto Chemical Co., Inc., 99.99%) was calcined in air at 1273 K for 10 h to remove moisture and carbonates. La_2O_3, La_2S_3 (Kojundo Chemical Laboratory Co., Ltd, 99.9%), Mg- and Al-codoped TiO_2, Cu_2S (Kojundo Chemical Laboratory Co., Ltd, 99%), Ag_2S (Kojundo Chemical Laboratory Co., Ltd, 99%) and sulfur (Kojundo Chemical Laboratory Co., Ltd, 99.99%) were mixed at a molar ratio of 2 : 3 : 4 : 0.9 : 0.1 : 0.5 in a N_2-filled glovebox. The precursor mixture was sealed in an evacuated quartz tube and heated from room temperature to 473 K in 9 min, from 473 to 673 K in 100 min, and from 673 to 1323 K in 53 h, and then maintained at 1323 K for 96 h. After the annealing process, the resulting solid chunk was ground into powder. The obtained Mg- and Al-codoped LTCA is denoted as LTCA for simplicity.

Fabrication of photocatalyst sheet

Photocatalyst sheets employing LTCA and GaN:ZnO as the HEP and OEP, respectively, were fabricated by the particle transfer method.[27,28] Briefly, LTCA and IrO_x-loaded GaN:ZnO (denoted as IrO_x-GaN:ZnO) (10 mg each) were suspended in 0.5 mL of 2-propanol. After sonication for a few minutes, the solution was dropcast onto a 3 × 3 cm glass plate. After the plate was dried at room temperature, an Au layer was deposited by vacuum evaporation (VFR-200 M/ERH, ULVAC) to a thickness of 0.3 μm. The plate was then heated at 523 K for 10 min in air to reduce the contact resistance between the particles and the Au layer. The primary glass plate was then attached to a second glass plate using adhesive carbon tape to peel off the powder/Au assembly, and then sonicated for a few seconds to remove the loosely bound particles to obtain a working photocatalyst sheet. To conduct Z-scheme water splitting reactions, the resulting sheet, denoted as LTCA/Au/IrO_x-GaN:ZnO, was successively loaded with Rh (0.1 μmol) and Cr_2O_3 (0.2 μmol as Cr) by photodeposition under visible light irradiation ($\lambda \geq 420$ nm) for 1 h each.

Characterisation of materials

The GaN:ZnO samples were analysed after washing with 0.5 M HNO_3 and calcining in air at 873 K, unless otherwise noted. X-ray diffraction (XRD) patterns were acquired using a Rigaku MiniFlex 300 with Cu Kα radiation operating at 30 kV and 10 mA. UV-vis diffuse reflectance spectroscopy (DRS) data were obtained using a spectrometer (V-670, JASCO) equipped with an integrating sphere. Scanning electron microscopy (SEM) images were captured using a Hitachi SU8000 system. TEM images and selected area electron diffraction (SAED) patterns were recorded using a JEOL JEM-2800. The cross-sectional sample for TEM observation was made by Ar ion milling using a JEOL EM-09100IS ion Slicer. Thermogravimetric analysis (TGA) measurements were performed using a Rigaku Thermo Plus TG 8120. The measurements were conducted by raising the temperature from room temperature to 1173 K at 10 K min^{-1} in ambient air. Energy-dispersive X-ray spectroscopy (EDS) was performed using an analytical system integrated with a desktop SEM instrument (Phenom Pharos, ThermoFisher Scientific). XPS analysis was carried out using a PHI Quantera II spectrometer with an Al Kα X-ray source. The binding energy was calibrated using the C 1s peak (285.0 eV) The bulk composition of the samples was analysed by inductively coupled plasma-atomic emission spectroscopy (ICP-AES, ICPS-8100, Shimadzu) and oxygen/nitrogen analysis (EMGA-620W, Horiba).

Photocatalytic reactions

Water splitting reactions were carried out in a Pyrex top-irradiation-type reaction vessel connected to a closed gas circulation system. The oxygen evolution reaction was performed using 0.1 g of IrO_x-loaded GaN:ZnO powder dispersed in an aqueous 30 mM $AgNO_3$ solution, while the hydrogen evolution reaction was performed using 0.1 g of Rh- and IrO_x-coloaded GaN:ZnO dispersed in an aqueous ascorbic acid (10 mM) or methanol (10 vol%) solution. The reactant solution was evacuated to remove air and irradiated with visible light ($\lambda \geq 420$ nm) from a 300 W Xe lamp equipped with a dichroic mirror and a cut-off filter after introduction of Ar (10 kPa) into the reaction

system. The reactor temperature was maintained at 283 K by circulating cooling water in the reactor jacket. The amount of evolved gases was analysed using a gas chromatograph (GC-8A, Shimadzu) equipped with Molecular Sieve 5A columns and a thermal conductivity detector.

The overall water splitting reaction was carried out using the same reaction system. Distilled water (40 mL) was added to the reactor, and a Cr_2O_3/Rh-loaded photocatalyst sheet was immersed. After degassing the reaction system thoroughly, the background pressure was adjusted to 5 kPa by introducing Ar. The photocatalyst sheet was illuminated with visible light ($\lambda \geq 420$ nm) from a 300 W Xe lamp or simulated sunlight generated by a solar simulator (HAL-320, Asahi Spectra Co., Ltd).

Apparent quantum yield measurement

The AQY for the oxygen evolution reaction was calculated as

$$\mathrm{AQY}(\%) = \frac{[A \times R]}{I} \times 100,$$

where A, R and I denote the number of electrons involved in the reaction, the number of gas molecules generated, and the number of incident photons in a given time span, respectively. In the oxygen evolution reaction from water, the value of A is 4 because it is a four-electron reaction. The oxygen evolution reaction was carried out in a 10 mM $AgNO_3$ aqueous solution and under irradiation from a Xe lamp equipped with a series of bandpass filters to produce monochromatic light. The number of incident photons was determined using a LS-100 spectroradiometer (EKO Instruments Co., Ltd). In the Z-scheme water splitting reaction using LTCA/Au/IrO_x-GaN:ZnO sheet, $A = 4$ and R is the rate of H_2 evolution. The coefficient of 4 reflects a two-step photoexcitation process to drive the hydrogen evolution reaction, which is a two-electron reaction. Z-scheme water splitting was carried out under the same conditions described in the previous section except for the use of a bandpass filter ($\lambda = 420$ nm) instead of a cut-off filter.

Solar-to-hydrogen energy conversion efficiency measurement

The STH efficiency for the photocatalyst sheet during Z-scheme water splitting was measured using the same experimental apparatus but with illumination from a solar simulator (HAL-320, Asahi Spectra Co., Ltd). The STH efficiency was calculated as

$$\mathrm{STH}(\%) = \frac{R(\mathrm{H_2}) \times \Delta G}{P \times S} \times 100,$$

where $R(H_2)$, ΔG, P, and S are the rate of hydrogen evolution from the Z-scheme water splitting system, the change in Gibbs free energy that accompanies water splitting, the energy intensity of the solar light irradiation, and the irradiation area (~6.25 cm^2), respectively. A value of 237 kJ mol^{-1} was used for ΔG_f, corresponding to the standard condition at 298 K. The energy intensity of the simulated sunlight (P) was adjusted to match that of Air Mass 1.5 Global (AM1.5 G) irradiance in the wavelength range of 350–800 nm and was assumed to be 100 mW cm^{-2}.

Conclusions

Porous but well-dispersed single crystal GaN:ZnO particles absorbing visible light up to 600 nm and exposing hexagonal crystal facets were synthesised in a sealed evacuated tube by using poorly crystalline δ-Ga_2O_3 as a raw material and adding metallic Zn to the starting materials. The Zn reacted with moisture generated from δ-Ga_2O_3 to form ZnO *in situ*, preventing oxidation of the nitriding reagents during the synthesis of GaN:ZnO. The *in situ* generated ZnO was incorporated into the GaN:ZnO material, increasing the ZnO content to about 65 mol%, which allowed extension of the visible light absorption edge to 600 nm. Moreover, the use of δ-Ga_2O_3 favored the growth of hexagonal prismatic GaN:ZnO particles by suppressing decomposition of the reactants and the associated production of inert byproducts.

The obtained GaN:ZnO evolved oxygen from an aqueous $AgNO_3$ solution with an AQY of 11.9% at 420 nm when loaded with an IrO_x cocatalyst. Moreover, IrO_x-GaN:ZnO acted as an OEP in a photocatalyst sheet for Z-scheme water splitting in combination with doped LTCA as a HEP and an Au thin film as a conductor layer. The resulting photocatalyst sheet exhibited a STH efficiency that was superior to that for a previously-reported Z-scheme suspension system using IrO_x-GaN:ZnO. There is still much room for clarification and optimization of the properties of GaN:ZnO and photocatalyst sheets containing it. This is expected to lead to improvements in the activity of photocatalytic sheets based on narrow bandgap nonoxide materials such as GaN:ZnO and LTCA.

Data availability

The data supporting this article have been included as part of the ESI.† Data are also available upon request from the authors.

Author contributions

T. H. and K. D. designed and supervised the research. N. I., H. S. and S. N. carried out the experiments. N. I., H. S., S. N., M. N., T. T., T. H. and K. D. discussed the results. N. I., S. N., T. H. and K. D. wrote the manuscript with contributions from the other authors.

Conflicts of interest

The authors declare no competing financial interests.

Acknowledgements

This research was supported by JST, PRESTO, Japan (grant no. JPMJPR20T9), the Artificial Photosynthesis Project (ARPChem) of the New Energy and Industrial Technology Development Organization (NEDO), Advanced Research Infrastructure for Materials and Nano-technology in Japan (ARIM)" of the Ministry of Education, Culture, Sports, Science and Technology (MEXT), Japan (Grant Number JPMXP1223UT0004), research equipment shared in MEXT Project for promoting public utilization of

advanced research infrastructure (program for supporting construction of core facilities, grant number JPMXS0441000024), and Mitsubishi Chemical Corporation. The authors thank Ms. Keiko Kato of The University of Tokyo and Ms. Michiko Obata of Shinshu university for their assistance with ICP-AES and XPS measurements.

Notes and references

1 M. R. Shaner, H. A. Atwater, N. S. Lewis and E. W. McFarland, A comparative technoeconomic analysis of renewable hydrogen production using solar energy, *Energy Environ. Sci.*, 2016, **9**, 2354–2371.

2 S. Nandy, S. A. Savant and S. Haussener, Prospects and challenges in designing photocatalytic particle suspension reactors for solar fuel processing, *Chem. Sci.*, 2021, **12**, 9866–9884.

3 Q. Wang, C. Pornrungroj, S. Linley and E. Reisner, Strategies to improve light utilization in solar fuel synthesis, *Nat. Energy*, 2022, **7**, 13–24.

4 H. Nishiyama, T. Yamada, M. Nakabayashi, Y. Maehara, M. Yamaguchi, Y. Kuromiya, Y. Nagatsuma, H. Tokudome, S. Akiyama, T. Watanabe, R. Narushima, S. Okunaka, N. Shibata, T. Takata, T. Hisatomi and K. Domen, Photocatalytic solar hydrogen production from water on a 100-m^2 scale, *Nature*, 2021, **598**, 304–307.

5 T. Hisatomi and K. Domen, Reaction systems for solar hydrogen production via water splitting with particulate semiconductor photocatalysts, *Nat. Catal.*, 2019, **2**, 387–399.

6 Z. Wang, Y. Inoue, T. Hisatomi, R. Ishikawa, Q. Wang, T. Takata, S. Chen, N. Shibata, Y. Ikuhara and K. Domen, Overall water splitting by Ta_3N_5 nanorod single crystals grown on the edges of $KTaO_3$ particles, *Nat. Catal.*, 2018, **1**, 756–763.

7 K. Chen, J. Xiao, J. J. M. Vequizo, T. Hisatomi, Y. Ma, M. Nakabayashi, T. Takata, A. Yamakata, N. Shibata and K. Domen, Overall Water Splitting by a $SrTaO_2N$-Based Photocatalyst Decorated with an Ir-Promoted Ru-Based Cocatalyst, *J. Am. Chem. Soc.*, 2023, **145**, 3839–3843.

8 Q. Wang, M. Nakabayashi, T. Hisatomi, S. Sun, S. Akiyama, Z. Wang, Z. Pan, X. Xiao, T. Watanabe, T. Yamada, N. Shibata, T. Takata and K. Domen, Oxysulfide photocatalyst for visible-light-driven overall water splitting, *Nat. Mater.*, 2019, **18**, 827–832.

9 R. Asai, H. Nemoto, Q. Jia, K. Saito, A. Iwase and A. Kudo, A visible light responsive rhodium and antimony-codoped $SrTiO_3$ powdered photocatalyst loaded with an IrO_2 cocatalyst for solar water splitting, *Chem. Commun.*, 2014, **50**, 2543–2546.

10 K. Maeda, T. Takata, M. Hara, N. Saito, Y. Inoue, H. Kobayashi and K. Domen, GaN:ZnO Solid Solution as a Photocatalyst for Visible-Light-Driven Overall Water Splitting, *J. Am. Chem. Soc.*, 2005, **127**, 8286–8287.

11 Y. Li, L. Zhu, Y. Yang, H. Song, Z. Lou, Y. Guo and Z. Ye, A Full Compositional Range for a $(Ga_{1-x}Zn_x)(N_{1-x}O_x)$ Nanostructure: High Efficiency for Overall Water Splitting and Optical Properties, *Small*, 2015, **11**, 871–876.

12 K. Maeda and K. Domen, Photocatalytic Water Splitting: Recent Progress and Future Challenges, *J. Phys. Chem. Lett.*, 2010, **1**, 2655–2661.

13 K. Liu, B. Zhang, J. Zhang, W. Lin, J. Wang, Y. Xu, Y. Xiang, T. Hisatomi, K. Domen and G. Ma, Synthesis of Narrow-Band-Gap GaN:ZnO Solid Solution for Photocatalytic Overall Water Splitting, *ACS Catal.*, 2022, **12**, 14637–14646.

14 R. Abe, Development of a New System for Photocatalytic Water Splitting into H_2 and O_2 under Visible Light Irradiation, *Bull. Chem. Soc. Jpn.*, 2011, **84**, 1000–1030.

15 H. Kato, Y. Sasaki, N. Shirakura and A. Kudo, Synthesis of highly active rhodium-doped $SrTiO_3$ powders in Z-scheme systems for visible-light-driven photocatalytic overall water splitting, *J. Mater. Chem. A*, 2013, **1**, 12327–12333.

16 R. Konta, T. Ishii, H. Kato and A. Kudo, Photocatalytic Activities of Noble Metal Ion Doped $SrTiO_3$ under Visible Light Irradiation, *J. Phys. Chem. B*, 2004, **108**, 8992–8995.

17 N. Iwasa, Z. Teng, G. Ma, T. Hisatomi and K. Domen, Synthesis of narrow bandgap gallium zinc nitride oxide solid solutions for photocatalytic water splitting under visible light, *Chem. Mater.*, 2024, **36**, 2917–2924.

18 K. Maeda and K. Domen, Solid Solution of GaN and ZnO as a Stable Photocatalyst for Overall Water Splitting under Visible Light, *Chem. Mater.*, 2010, **22**, 612–623.

19 A. Sharma, M. Varshney, H. Saraswat, S. Chaudhary, J. Parkash, H. J. Shin, K. H. Chae and S. O. Won, Nano-structured phases of gallium oxide (GaOOH, α-Ga_2O_3, β-Ga_2O_3, γ-Ga_2O_3, δ-Ga_2O_3, and ε-Ga_2O_3): fabrication, structural, and electronic structure investigations, *Int. Nano Lett.*, 2020, **10**, 71–79.

20 X. Liu, C. Wessel, F. Pan and R. Dronskowski, Synthesis and single-crystal structure determination of the zinc nitride halides Zn_2NX (X=Cl, Br, I), *J. Solid State Chem.*, 2013, **203**, 31–36.

21 Z. Li, L. Zhang, Y. Liu, C. Shao, Y. Gao, F. Fan, J. Wang, J. Li, J. Yan, R. Li and C. Li, Surface-Polarity-Induced Spatial Charge Separation Boosts Photocatalytic Overall Water Splitting on GaN Nanorod Arrays, *Angew. Chem., Int. Ed.*, 2020, **59**, 935–942.

22 M. Huang, J. Lian, R. Si, L. Wang, X. Pan and P. Liu, Spatial Separation of Electrons and Holes among ZnO Polar {0001} and $\{10\bar{1}0\}$ Facets for Enhanced Photocatalytic Performance, *ACS Omega*, 2022, **7**, 26844–26852.

23 Y. Chen, H. Zhao, B. Liu and H. Yang, Charge separation between wurtzite ZnO polar {001} surfaces and their enhanced photocatalytic activity, *Appl. Catal., B*, 2015, **163**, 189–197.

24 M. W. Liao, H. T. Jeng and T. P. Perng, Formation Mechanism and Bandgap Reduction of GaN–ZnO Solid-Solution Thin Films Fabricated by Nanolamination of Atomic Layer Deposition, *Adv. Mater.*, 2023, **35**, 2207849.

25 K. Maeda, K. Teramura and K. Domen, Effect of post-calcination on photocatalytic activity of $(Ga_{1-x}Zn_x)(N_{1-x}O_x)$ solid solution for overall water splitting under visible light, *J. Catal.*, 2008, **254**, 198–204.

26 S. Nandy, T. Hisatomi, M. Nakabayashi, H. Li, X. Wang, N. Shibata, T. Takata and K. Domen, Oxide layer coating

enabling oxysulfide-based photocatalyst sheet to drive Z-scheme water splitting at atmospheric pressure, *Joule*, 2023, **7**, 1641–1651.

27 Q. Wang, Y. Li, T. Hisatomi, M. Nakabayashi, N. Shibata, J. Kubota and K. Domen, Z-scheme water splitting using particulate semiconductors immobilized onto metal layers for efficient electron relay, *J. Catal.*, 2015, **328**, 308–315.

28 T. Minegishi, N. Nishimura, J. Kubota and K. Domen, Photoelectrochemical properties of $LaTiO_2N$ electrodes prepared by particle transfer for sunlight-driven water splitting, *Chem. Sci.*, 2013, **4**, 1120–1124.